ACS APPLIED MATERIALS & INTERFACES

Research Article

www.acsami.org

Controlled van der Waals Epitaxy of Monolayer MoS_2 Triangular Domains on Graphene

Hiroki Ago,*[,†,‡,§] Hiroko Endo,[†] Pablo Solís-Fernández,[†] Rina Takizawa,[‡] Yujiro Ohta,[‡] Yusuke Fujita,[‡] Kazuhiro Yamamoto,[†] and Masaharu Tsuji[†,‡]

[†]Institute for Materials Chemistry and Engineering (IMCE) and [‡]Graduate School of Engineering Sciences, Kyushu University, Fukuoka 816-8580, Japan

[§]PRESTO, Japan Science and Technology Agency (JST), Saitama 332-0012, Japan

Supporting Information

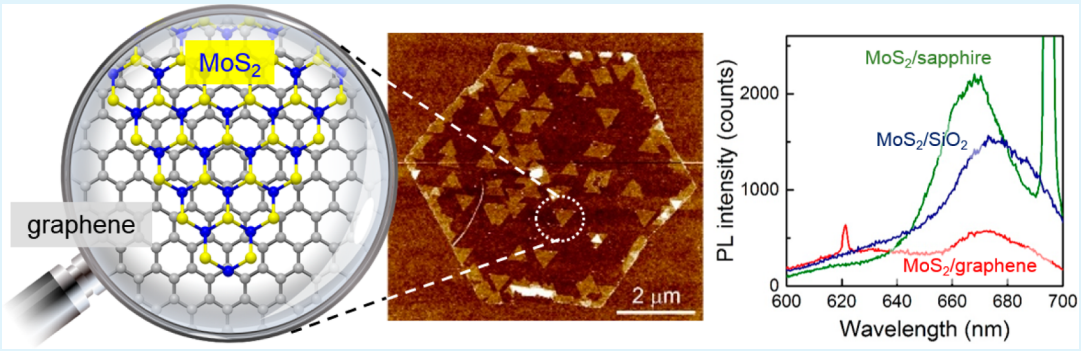

ABSTRACT: Multilayered heterostructures of two-dimensional materials have recently attracted increased interest because of their unique electronic and optical properties. Here, we present chemical vapor deposition (CVD) growth of triangular crystals of monolayer MoS_2 on single-crystalline hexagonal graphene domains which are also grown by CVD. We found that MoS_2 grows selectively on the graphene domains rather than on the bare supporting SiO_2 surface. Reflecting the heteroepitaxy of the growth process, the MoS_2 domains grown on graphene present two preferred equivalent orientations. The interaction between the MoS_2 and the graphene induced an upshift of the Raman G and 2D bands of the graphene, while significant photoluminescence quenching was observed for the monolayer MoS_2. Furthermore, photoinduced current modulation along with an optical memory effect was demonstrated for the MoS_2−graphene heterostructure. Our work highlights that heterostructures synthesized by CVD offer an effective interlayer van der Waals interaction which can be developed for large-area multilayer electronic and photonic devices.

KEYWORDS: *MoS_2, graphene, van der Waals epitaxy, CVD, interface*

INTRODUCTION

The recent development of graphene research has opened a new field of atomically thin, two-dimensional (2D) layered materials.[1−4] In addition to graphene with its zero-gap character, other 2D materials, such as transition metal dichalcogenides (TMDCs), hexagonal boron nitride (h-BN), and more recently phosphorene have attracted increased interest. These new materials possess electronic structures completely different from that of graphene, thus offering a wide range of physical properties.[1−5] Moreover, the integration of two or more of these layered 2D materials is expected as a new promising direction to achieve novel electronic and optical properties.[6] In addition to their electronic properties, heterostructures of layered materials can also afford high optical transparency as well as good mechanical flexibility due to their atomic-level thickness.[7]

Graphene has an extremely high carrier mobility and high electrical conductivity, which promise applications in many electronic devices. However, it possesses a low optical absorption in the visible light range and is a gapless material.[8,9] On the other hand, monolayer MoS_2 has a band gap of 1.9 eV and shows high optical absorption as well as clear photoluminescence (PL) in the visible region.[10,11] Accordingly, the MoS_2-based field-effect transistors (FETs) show high on/off ratios (>10^6) due to their large band gap.[12] Thus, it is expected that in heterostructures of graphene and MoS_2 both materials can complement each other, which could, for example, add high optical response to graphene FETs. Recently, new optoelectronic devices and unique phenomena based on the interaction between these two materials, such as high gain photodetectors, photoresponsive memory devices, and gate-tunable photocurrent generation, have been developed.[13−15] Logic transistors

Received: December 4, 2014
Accepted: February 19, 2015
Published: February 19, 2015

DOI: 10.1021/am508569m
ACS Appl. Mater. Interfaces 2015, 7, 5265−5273

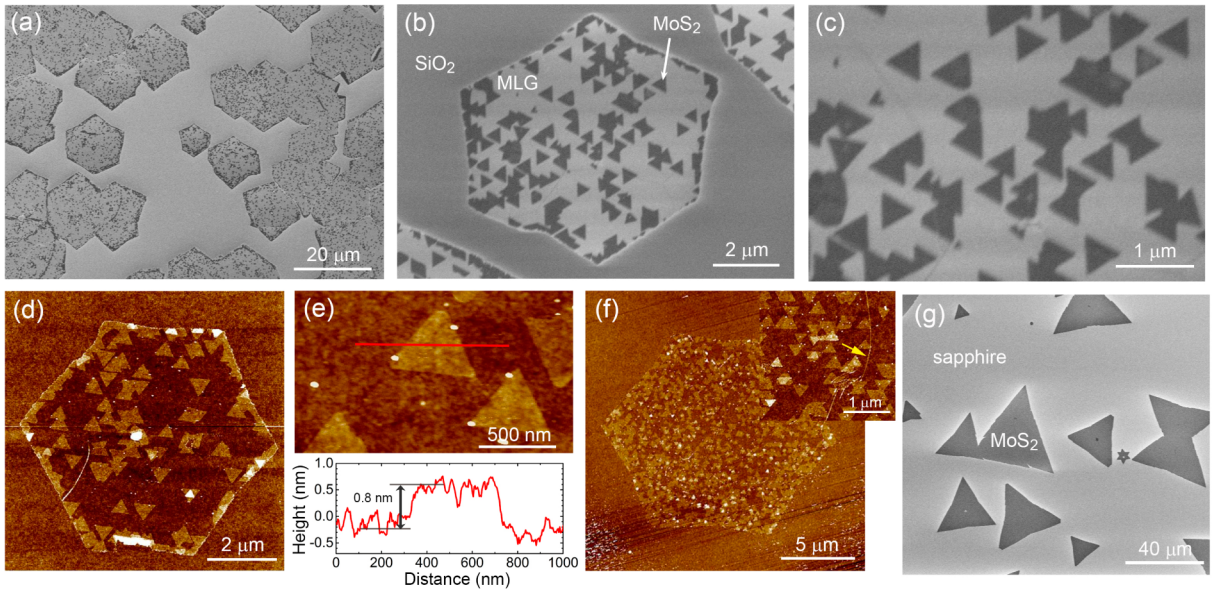

Figure 1. SEM (a–c) and AFM (d–f) images of single-crystalline MoS_2 domains grown on hexagonal graphene domains. (Lower panel of e) Height profile of a MoS_2 domain along the red line. (f) High-density MoS_2 on a MLG domain. (Inset of f) Magnified image, and the arrow shows a wrinkle of the underlying graphene. (g) SEM image of MoS_2 domains grown on a *c*-plane sapphire substrate.

and nonvolatile memories have also been demonstrated using graphene–MoS_2 heterostructures.[16,17] However, most of the previous attempts to prepare such heterostructures rely on the mechanical exfoliation and/or transfer of at least one of the two materials, either the graphene or the MoS_2.[7,13−18] Large-area monolayer graphene (MLG) can be grown by chemical vapor deposition (CVD), and exfoliated MoS_2 flakes have been transferred onto the MLG.[15−17] The CVD-grown MLG was also transferred onto exfoliated MoS_2 flakes or a single crystal of MoS_2 to investigate the interface interaction.[18,19] The drawback of using mechanically exfoliated MoS_2 crystals is their limited flake sizes and the inability to control the number of layers. Recent developments in the CVD growth of monolayer MoS_2 have enabled the large-area fabrication of devices,[20−22] and CVD–graphene has been successfully stacked onto CVD–MoS_2 by a wet-transfer technique.[13] However, in each of these previous works the heterostructures have been formed by bringing the different materials into contact using transfer processes. Thus, it is likely that these heterostructures suffer from the presence of impurities in the interface, such as hydrocarbons,[23] mainly trapped during the transfer process. The presence of these impurities has a negative impact on the properties of the heterostructures by reducing the interlayer coupling. Consequently, it has been pointed out that the barrier height for the vertical conduction in MoS_2–graphene heterostructures prepared by multiple transfer is significantly affected by the quality of the interface, which can result in a large barrier height between the transferred layers.[24]

Therefore, it is important to grow the second layer on the first one for the study of the interface interaction. Also, CVD growth is preferable for the development of large-scale production of multilayered heterostructures for future device applications. Some works have been published on the CVD growth of MoS_2 over graphene templates prepared by CVD,[25] mechanical exfoliation,[26] and thermal annealing of SiC substrates.[27] Although these works demonstrated an epitaxial relationship between the MoS_2 and the underlying graphene, the structure and orientation of MoS_2 domains were not controlled.[25−27] Similar to the MoS_2, monolayer $MoSe_2$ was also grown on graphene by CVD but the shape and orientation of $MoSe_2$ were not controlled.[28] The CVD growth of triangular WS_2 was also demonstrated on h-BN, but small flakes of exfoliated h-BN were used as a growth substrate.[29] Recently, other materials such as single-crystalline GaN sheets and inorganic nanowires ($In_xGa_{1-x}As$) have been also epitaxially grown on graphene.[30,31]

In this paper, we demonstrate the direct CVD growth of single-crystal domains of monolayer MoS_2 over CVD-grown hexagonal graphene domains. We show that the growth of MoS_2 proceeds by van der Waals epitaxy, i.e., single-crystalline MoS_2 growth on single-crystalline graphene with controlled orientation. It was also found that MoS_2 can be selectively grown on the graphene without depositing on the bare SiO_2 supporting substrate. The electronic interaction between MoS_2 and graphene was studied by Raman and PL spectroscopies and by carrier transport measurements. In contrast with the observations made for stacked films which were prepared by multiple transfer, we found an upshift of the graphene G and 2D Raman bands and a strong quenching of PL from the monolayer MoS_2. Furthermore, a clear optical memory effect accompanied by photoinduced current modulation was demonstrated using our MoS_2–graphene heterostructures.

RESULTS AND DISCUSSION

Figure 1a–f shows scanning electron microscope (SEM) and atomic force microscope (AFM) images of MoS_2 grown on MLG. The hexagonal graphene domains were grown by ambient pressure CVD at 1075 °C on a crystalline Cu(111) thin film deposited on *c*-plane sapphire using a previously reported method.[32] After transferring the hexagonal MLG domains onto a SiO_2/Si substrate, MoS_2 crystals were grown on the MLG by a second CVD process using MoO_3 and S powder as precursors. The experimental setup for the growth of the MoS_2 is schematically illustrated in the Supporting Information, Figure S1, while detailed experimental conditions are described in the Experimental Section. Briefly, after heating the graphene

DOI: 10.1021/am508569m
ACS Appl. Mater. Interfaces 2015, 7, 5265−5273

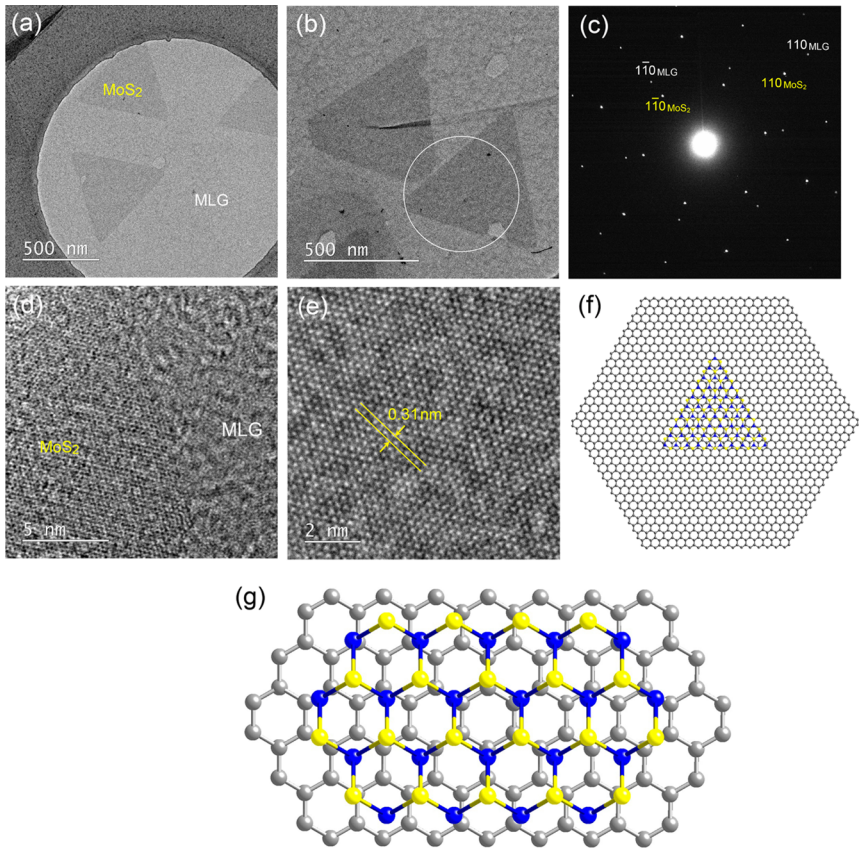

Figure 2. (a and b) TEM images of MoS_2 crystals grown on MLG. (c) SAED pattern of the MoS_2/graphene taken at the region marked in b. (d and e) High-resolution TEM images. (f and g) Atomic models of MoS_2 on graphene determined from the SAED pattern and SEM images. Blue, yellow, and gray atoms represent Mo, S, and C atoms, respectively.

to 900−960 °C, the MoO_3 and S feedstocks were heated to 630−650 and 165 °C, respectively, for 1 h under an Ar flow. In several previous reports, MoS_2 was grown on a SiO_2/Si substrate set just above the MoO_3 powder. However, in our case the graphene substrate and the MoO_3 were placed separately in order to control the temperature of the graphene substrate independently, as this parameter was found to be important for effective growth of MoS_2 on graphene.

Interestingly, we found that MoS_2 preferentially grows on the MLG domains, while few MoS_2 domains were observed on the surface of the supporting SiO_2 as seen in Figure 1a and 1b. The MoS_2 domains grown on the graphene hexagons present triangular shapes with lateral sizes ranging from ∼200 nm to ∼1 μm (Figure 1b and 1c). The triangular MoS_2 domains have two dominant orientations, with their sides always parallel to one of the sides of the supporting graphene hexagonal domain, suggesting the epitaxial growth of MoS_2 on MLG.

Figure 1d shows an AFM image of a different graphene domain. It is also seen that MoS_2 preferentially grows on the graphene surface, while no MoS_2 domains appear on the SiO_2 surface. The density of MoS_2 domains on the sides (edges) of the graphene domain is higher than that found inside of the graphene domain. It is likely that MoS_2 precursors deposited on the SiO_2 surface migrate to the sides of a graphene domain, and then MoS_2 domains start to nucleate at the sides. Desorption of the MoS_2 precursors might also occur more frequently on SiO_2 than on graphene. The height profiles of the MoS_2 domains measured by AFM (Figure 1e) show a height difference of about 0.8 nm with respect to the underlying graphene, which is close to the reported height of monolayer MoS_2 (0.72 nm).[33] The growth of monolayer MoS_2 was also confirmed by Raman and photoluminescence (PL), as discussed later. By controlling the growth conditions, such as increasing the MoO_3 temperature or putting the graphene substrate closer to the feedstock, we can increase the density of triangular MoS_2 domains on graphene. For example, increasing the MoO_3 temperature from 630 (Figure 1a−e) to 650 °C (Figure 1f) increased the MoS_2 coverage of graphene domains. In the inset of Figure 1f, one can clearly see a wrinkle which originated from the graphene, proving that the graphene remains underneath the MoS_2 domains. Figure S2, Supporting Information, shows the dependence of the distance between the MoO_3 feedstock and the graphene substrate. Graphene domains fully covered with MoS_2 can be obtained at the positions close to the MoO_3, though multilayer MoS_2 was partly observed (Figure S2c, Supporting Information). Further decrease of the distance to the MoO_3 gave the graphene fully covered with multilayer MoS_2 (Figure S2d, Supporting Information). In these samples, however, the SiO_2 surface was also partially covered with MoS_2, though clear triangular structures were not frequently observed.

To verify the role of the graphene on the epitaxial growth of MoS_2, we also used a sapphire *c*-plane substrate instead of graphene/SiO_2/Si. When using the sapphire substrate, large triangular MoS_2 domains with lateral sizes over 30 μm were observed (Figure 1g). Although the MoS_2 domain size on sapphire was much larger than that on graphene, these triangle MoS_2 domains were not aligned in the same direction. At this moment there is an ongoing discussion on the orientation of

DOI: 10.1021/am508569m
ACS Appl. Mater. Interfaces 2015, 7, 5265−5273

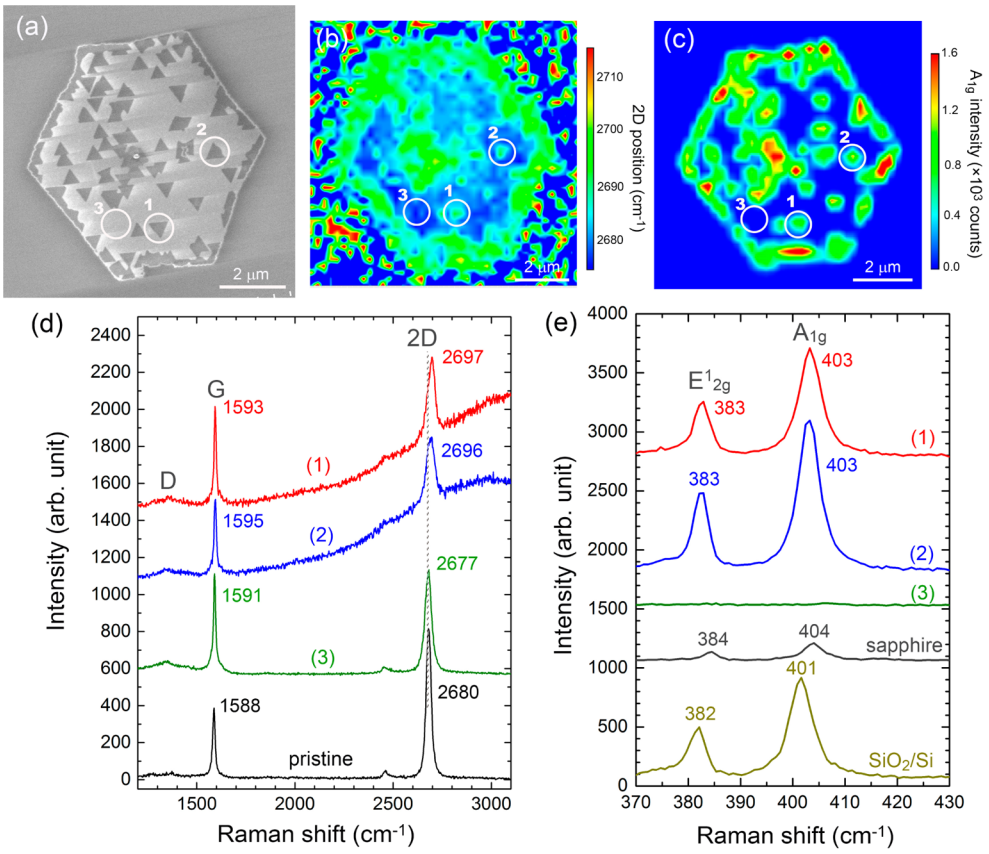

Figure 3. SEM image of a MoS_2−graphene heterostructures (a), and corresponding Raman mapping images of the peak position of the 2D band of graphene (b) and the peak intensity of the A_{1g} mode of MoS_2 (c). (d) Graphene wavenumber region of the Raman spectra at the areas marked in a−c and spectrum of pristine graphene measured before MoS_2 growth. (e) MoS_2 wavenumber region of the Raman spectra. For comparison, spectra of a small MoS_2 domain with 0.5−1 μm size grown on sapphire and then transferred on SiO_2/Si were also measured.

triangular MoS_2 domains on *c*-plane sapphire.[34−36] While Dumcenco et al. demonstrated the CVD growth of orientation-controlled MoS_2 domains on sapphire,[34] Wu et al. reported uncontrolled orientation of the MoS_2 grown on sapphire.[35] More recently, Ji et al. found that at the commonly employed growth temperatures, triangular MoS_2 domains possess two main orientations (30° apart) together with their 180°-rotated ones.[36] In addition, these orientations were reported to have a broad Gaussian distribution.[36] Overall, it is likely that the orientation of MoS_2 crystals depends on the CVD conditions, such as temperature and pressure, as well as surface conditions of sapphire and that it is not straightforward to grow perfectly aligned MoS_2 on sapphire. Because we did not observe the aligned growth, it is difficult for us to discuss the most important factor which determines the MoS_2 orientation. However, it is worth noting that under a relatively wide range of reaction conditions, MoS_2 domains are highly oriented on the CVD graphene domains (see Figure 1b−d), signifying an effective interlayer coupling between these two layered materials.

The structure of the MoS_2−graphene heterostack was further studied by transmission electron microscopy (TEM). Figure 2a and 2b shows TEM images of MoS_2 supported on graphene. Triangular MoS_2 domains with the two distinct orientations can be seen on the graphene. We note that no impurities are seen near the MoS_2 domains in the TEM images. We determined the relative orientation of the MoS_2 and graphene by measuring selected-area electron diffraction (SAED) from the area marked in Figure 2b. In the SAED pattern shown in Figure 2c, two sets of hexagonal diffraction patterns with an identical orientation can be seen, originating from the MoS_2 and the graphene. This result indicates that both MoS_2 and graphene have high crystallinity and that the orientations of their hexagonal lattices match completely. Due to the larger lattice constant of the MoS_2 (a = 0.312 nm) compared to that of graphene (a = 0.246 nm), the diffraction spots from MoS_2 locate closer to the center beam. Note that no circular patterns were observed in the SAED, implying the absence of contaminants, such as amorphous carbon, residual MoO_3/S feedstock, and PMMA residue.

High-magnification TEM images shown in Figure 2d and 2e also confirmed the growth of crystalline MoS_2, with a lattice constant estimated from the TEM image (~0.31 nm), which is consistent with that of MoS_2 (a = 0.312 nm). Figure 2f and 2g depicts the atomic structures of triangular MoS_2 grown on hexagonal graphene domains, determined based on our SEM and TEM measurements. The orientations of the hexagonal networks of MoS_2 and graphene matched well, proving that the growth is based on van der Waals epitaxy. As can be deduced from the symmetry shown in Figure 2g, a relative rotation of 180° between the MoS_2 and the graphene gives a completely equivalent structure. This accounts for the two orientations of the triangular MoS_2 domains observed in Figures 1c, 1d, and 2a; both configurations are essentially the same. Therefore, we observed two main orientations for the MoS_2 domains grown on the CVD graphene. Because this epitaxy was not observed

DOI: 10.1021/am508569m
ACS Appl. Mater. Interfaces 2015, 7, 5265−5273

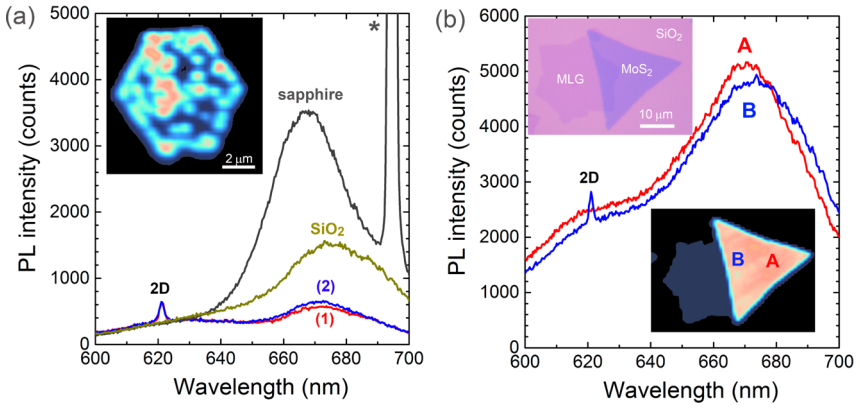

Figure 4. (a) PL spectra of MoS_2 grown on graphene (red and blue) and sapphire (black). Spectra 1 and 2 were taken at the positions marked in Figure 3a. PL spectra of MoS_2 grown on sapphire (black) and after transfer to a SiO_2/Si substrate (brown) are also shown. Asterisk (*) and 2D indicate peaks from a sapphire substrate and graphene 2D band, respectively. (Inset) PL intensity mapping (660−680 nm) of the same MLG domain with MoS_2 of Figure 3a. (b) PL spectra of MoS_2−graphene heterostack prepared by multiple transfer; hexagonal MLG domains were transferred on a SiO_2/Si substrate, followed by the second transfer of triangle MoS_2 domains from sapphire. (Upper and lower insets) Optical micrograph and PL intensity mapping of the heterostack, respectively. Spectra A and B were taken at the positions marked in the PL mapping image.

for the MoS_2 on the sapphire *c*-plane in our system (see Figure 1g), it is likely that the hexagonal lattice of graphene plays an essential role in the growth of MoS_2 crystals.

We measured the Raman spectra of the heterostructure, since Raman spectroscopy is a powerful tool to analyze both graphene and MoS_2. Figure 3a shows an SEM image of the same hexagonal graphene domain shown in Figure 1d, which is partly covered with triangular MoS_2 domains. In Figure 3d Raman spectra measured at the points marked as 1, 2, and 3 in Figure 3a are compared with that of pristine graphene. The Raman spectrum of the pristine graphene collected before MoS_2 growth (bottom spectrum) showed sharp G and 2D bands with negligible D band. The 2D band, located at 2680 cm^{-1}, presents a narrow full width at half-maximum (fwhm) of 30−35 cm^{-1} and a high relative intensity with respect to the G band ($I_{2D}/I_G \approx 2$). These results prove the growth of high-quality monolayer graphene.[32,37] After the CVD growth of MoS_2, the bare graphene area (spectrum 3 in Figure 3d) showed a reduction of the 2D band intensity due to the high-temperature growth process in Ar. It is known that the thermal annealing of MLG can reduce the I_{2D}/I_G ratio, mainly due to a modification of the interaction between the graphene and the underlying SiO_2.[38] A D band appeared after MoS_2 growth, but its intensity is still weak, suggesting that the graphene domain maintains high quality even after the MoS_2 CVD process.

The Raman spectrum of the graphene underneath MoS_2 domains showed clear differences from that of the bare graphene area, as seen in spectra 1 and 2 of Figure 3d. First, a broad background which increases with higher wavenumbers was observed. This background is originated in the PL of the MoS_2, which confirms the presence of both graphene and MoS_2 in the measured area. Second, the intensity of the 2D band was suppressed by MoS_2. Finally, both the G and the 2D bands upshifted when compared with the bare graphene area (spectrum 3). In Figure 3b, the spatial distribution of the 2D peak position is mapped for the same graphene domain shown in Figure 3a. It can be seen that the areas of graphene covered with MoS_2 show an upshift in the 2D band, while for the bare graphene the 2D band stays below 2680 cm^{-1}. There are several factors that influence the Raman 2D band position: temperature, charge transfer, and strain.[39−44] In our Raman measurements, the spectra were taken at room temperature and the laser power was set low to avoid the influence of the laser heating. Thus, the observed 2D-band upshift does not originate in differences of temperature. It is known that the I_{2D}/I_G ratio is sensitive to the carrier doping; the I_{2D}/I_G ratio decreases with increasing doping level. Also, depending on the introduced carriers the 2D-band position shifts differently, with up- and downshifts corresponding to hole and electron doping, respectively.[39−41] We can exclude the effect of reaction of graphene with MoO_3 or S, as bare graphene area shows a smaller shift compared with the MoS_2-covered area. Our observation of the upshift of G and 2D band is different from that found in the previous literature, which reports a downshift for the transferred MoS_2−graphene stacks.[13,18] This downshift was explained by the photoinduced electron transfer from MoS_2 to graphene,[13,18] thus leading to an n-type doping of the latter. However, a recent work reports the upshift of the 2D band even for mechanically stacked heterostructures, which is explained by the interlayer coupling between graphene and MoS_2.[45] Since Raman spectroscopy uses visible light, the influence of the laser emission is important for the present system. As we will discuss later, the photoinduced electron transfer was also observed for our MoS_2−graphene heterostructures.

There is a possibility that mechanical strain also modifies the Raman shift of graphene.[39−42] Since MoS_2 and graphene have positive and negative thermal expansion coefficients (TEPs), respectively (MoS_2 = 1.9 × 10^{-6} K^{-1}, graphene ≈ −8 × 10^{-6} K^{-1}),[46,47] it is likely that the MoS_2 domains formed at high temperature (typically 900−960 °C) lead to a compressive strain in the graphene after cooling down to room temperature. The estimated compressive strain calculated from the above TEP values is ∼0.9% when cooled down from 900 °C. The strain calculated from the Raman 2D band shift ($\Delta\omega_{2D}$ = 20 cm^{-1}) is 0.3%, based on our previously determined factor of $\partial\omega_{2D}/\partial\varepsilon$ = −72 cm^{-1}/% for 2D band.[48] This discrepancy may come from slippage of MoS_2, wrinkle formation in graphene, and/or the contact of graphene to SiO_2 substrate surface. Considering a recent report on the graphene/MoS_2 heterostack,[45] we assume that the effective interlayer coupling with the MoS_2 domains and strain effect due to the high temperature during the CVD contribute to the observed upshift of the

DOI: 10.1021/am508569m
ACS Appl. Mater. Interfaces 2015, 7, 5265−5273

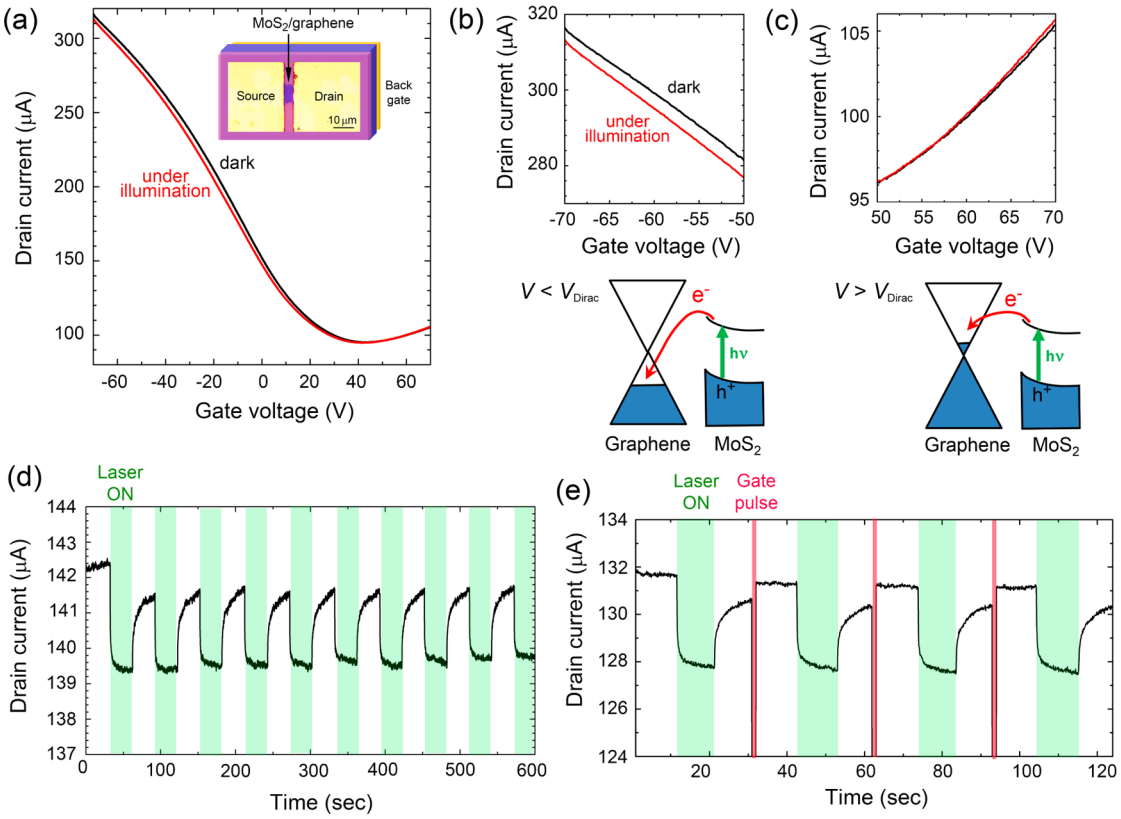

Figure 5. (a–c) Transfer curves of the graphene FET covered with MoS_2 measured in the dark (black curve) and under illumination of a 532 nm laser (red curve). (Inset of a) Schematic of device structure with a channel width 5 μm. (b and c) Magnified curves at low and high gate voltages, respectively. Band diagrams explaining the photoinduced electron transfer for each gate voltage are also illustrated. (d) Photoresponse of the drain current measured under illumination with a laser during 30 s intervals (gate and drain voltages are set −40 and 0.1 V, respectively). Green shows the period of the light illumination. Note that the current does not reach the initial original current after the photoinduced current modulation. (e) Recovery of the initial current by applying short positive gate voltage pulses (70 V) during the laser off period (gate voltage is 0 V except for the short pulse, and drain voltage is 0.1 V).

Raman G and 2D bands of the graphene, but further study is necessary for deeper understanding of the interface interaction.

Raman spectra in the wavenumber region where MoS_2 becomes active were also measured, as displayed in Figure 3e. The MoS_2 domains on CVD graphene showed two main Raman peaks, the A_{1g} peak associated with out-of-plane vibration and the E^1_{2g} peak associated with in-plane vibration, located at 403 and 383 cm^{-1}, respectively (see spectra 1 and 2 of Figure 3e). The separation between these two peaks (20 cm^{-1}) indicates the growth of monolayer MoS_2.[21,24,35] The intensity of the Raman A_{1g} band is mapped in Figure 3c for the same graphene domain depicted in Figure 3a. It is clear that the intensity distribution is consistent with the distribution of MoS_2 seen in the SEM image (see Figure 3a), while none of the MoS_2-related peaks were observed on bare graphene area (spectrum 3). Multilayer MoS_2 areas such as those present at the center of graphene domains showed the highest Raman intensity for the MoS_2 peaks, with the peak separation increased to 22–23 cm^{-1}. Raman spectra were also collected for MoS_2 domains grown on sapphire before and after being transferred onto SiO_2 for comparison. For reliable comparison, spectra were taken on MoS_2 domains of similar lateral sizes (~0.5–1 μm) for three different substrates. The intensities of A_{1g} and E^1_{2g} peaks on sapphire are weaker than those on graphene, but they became stronger after transferring onto SiO_2.

Reflecting the band structure change from indirect band gap semiconductor of bulk MoS_2 to direct gap semiconductor in monolayer MoS_2, a strong PL appears when the number of MoS_2 layers is reduced to one.[10] Shown in Figure 4a are the PL spectra of MoS_2 domains grown on graphene and sapphire and of MoS_2 transferred on SiO_2 from sapphire. MoS_2 domains with similar sizes were investigated in the three cases. It turned out that the PL intensity is strongly suppressed for the MoS_2–graphene heterostructure. The PL intensity of monolayer MoS_2 on graphene was significantly reduced by 50–70% when compared with that of monolayer MoS_2 on SiO_2, while the PL quenching is >70% when compared with the MoS_2 grown on sapphire. Such strong quenching of the luminescence from the MoS_2 grown on graphene proves that there exists a strong electronic interaction between the graphene and the photoexcited MoS_2. It should be noted that, according to previous reports, the PL intensity of monolayer MoS_2 located below transferred CVD graphene is reduced only by ~20–30%.[13,18] Therefore, our MoS_2 domains directly grown on graphene are more strongly affected by the underlying graphene, suggesting the importance of direct growth for effective interlayer coupling. Such strong PL quenching was also reported for the $MoSe_2$ directly grown on graphene, though the structure of $MoSe_2$ domains was not well defined.[28]

To further investigate the efficacy of the direct heteroepitaxial CVD growth, MoS_2–graphene heterostacks were also prepared by transferring large MoS_2 domains grown on sapphire onto a graphene/SiO_2 substrate for comparison. The upper inset of Figure 4b shows an optical image of one of such

DOI: 10.1021/am508569m
ACS Appl. Mater. Interfaces 2015, 7, 5265–5273

stacks in which the transferred MoS_2 and the graphene overlap in a small area. The PL mapping image (Figure 4b lower inset) indicates that the presence of graphene does not strongly influence the PL intensity of the MoS_2. Correspondingly, the individual PL spectra collected at point B (overlapped region) and at point A (MoS_2 directly on top of the SiO_2 substrate) show that in the overlapped area the intensity of the PL is decreased only by 6% compared to regions at which the MoS_2 is in contact with the SiO_2. This decrease is much smaller than that observed for the CVD-grown MoS_2 on graphene (50−70%). This result indicates that the effective interlayer coupling is much stronger when the MoS_2 is directly grown on the graphene than in the case when it is transferred. It should be noted that the PL intensities in Figure 4b are higher than those shown in Figure 4a due to the larger size of the MoS_2 domain used.

In order to rule out the presence of interlayer contaminants in the CVD-grown MoS_2−graphene heterostructure, the surface cleanness of the graphene surface was inspected by AFM, as shown in Figure S3, Supporting Information. The surface images of the as-transferred graphene domains on SiO_2 taken after dissolving the PMMA by acetone suggest that some polymer residues remain on the graphene surface. The sample was then subjected to the same annealing process used for the CVD growth of MoS_2 (heat at 960 °C under an Ar flow) but without the presence of the MoO_3 and S precursors. The AFM data show a significant reduction of the PMMA residue due to this annealing process. Also, polymer residues were absent in the high-resolution TEM images (Figure 2d and 2e) of the MoS_2−graphene stacks. Therefore, we conclude that removal of the PMMA residue during the CVD ensures a clean MoS_2−graphene interface, inducing the observed enhancement of their coupling, resulting in a controlled domain orientation.

To avoid the issues of polymer residues, the possibility of a direct growth of MoS_2 over as-grown graphene on Cu(111)/sapphire was also studied. As the graphene does not undergo transfer to an SiO_2 substrate prior to the MoS_2 growth, this approach can potentially avoid the issues of PMMA contamination. However, as shown in Figure S4, Supporting Information, we found that at the temperatures employed for the CVD growth of the MoS_2 the Cu substrate strongly reacts with the sulfur present in the chamber, making the Cu(111) film look black and its surface very rough. After transfer to SiO_2 for better examination, large particles and flakes of multilayer MoS_2 can be seen, but the growth of monolayer MoS_2 on graphene domains was not confirmed. Although Cu degradation can be avoided by changing the precursor source,[25] these approaches suffer from decreased control of the MoS_2 orientation. Therefore, currently the direct growth of MoS_2 on transferred graphene is the most reliable and scalable method to synthesize clean and controlled MoS_2−graphene heterostructures.

Transport properties of the MoS_2−graphene heterostructure were measured by fabricating back-gated field-effect transistors (FETs) on a SiO_2/Si substrate (Figure 5). For FETs, MLG domains fully covered with MoS_2 were used. Results of other devices with different MoS_2 coverage are also presented in Figures S5 and S6, Supporting Information. The presence of MoS_2 domains over a MLG domain is expected to add photosensitivity to the graphene FET. This is because MoS_2 has strong optical absorption (1×10^7 m^{-1}) for the visible light (band gap of monolayer MoS_2 is 1.9 eV),[11] while graphene has a very low optical absorbance (2.3% for visible light).[9] As shown in Figure 5a, a decrease of the drain current of the MoS_2−graphene device was observed at gate voltages below the Dirac point (~40 V) upon illumination with a 532 nm laser beam with a power density of 140 W/m^2. The decrease of the drain current can be more clearly seen in Figure 5b. The photoinduced current modulation was about 2%. On the other hand, a slight increase of the drain current was seen at gate voltages higher than the Dirac point (Figure 5c).

These optical responses of the MoS_2−graphene heterostructure can be explained by a photoinduced electron transfer from MoS_2 to graphene, as illustrated in Figure 5b and 5c. At gate voltages below the Dirac point, drain current in the graphene FET is dominated by holes which are accumulated by the gate voltage. However, when the FET is illuminated with visible light the current is reduced due to the injection of photoinduced electrons from MoS_2 to graphene. On the other hand, under a gate voltage higher than the Dirac point, the drain current is dominated by electrons. Thus, the increased current upon illumination can be accounted for by the increase of the carrier electron density due to photoexcited electron transfer. The amount of the current increase remains small due to a low degree of electron transfer, as the Fermi energy of graphene reaches a value close to the energy level of the conduction band of MoS_2. It should be noted that the photoresponse was seen even under zero gate voltage. Therefore, the PL quenching observed in the directly grown MoS_2 on graphene (see Figure 4a) can be originated in electron transfer from MoS_2 to graphene, which hinders the recombination of electron−hole pairs created by the photoexcitation.

The photoinduced current modulation is repeatable, as shown in Figure 5d. However, the current did not immediately recover to its original value once the laser is switched off. This is explained by the trapping of positive charge in MoS_2 domains due to the photoexcited electron transfer. This positively charged MoS_2 can be recovered by applying a gate voltage larger than the Dirac point for a short period of time, which supplies electrons to the MoS_2 layer to compensate for the excessive positive charge. As demonstrated in Figure 5e, a pulse of the positive gate voltage (+70 V for 1 s) recovered the drain current to the initial value. In this regard, the MoS_2−graphene heterostructure can be used as an optical memory device. A similar effect was observed for vertical stacks of multilayer MoS_2 sheets made by exfoliation with graphene,[14] but here we demonstrate it for the directly grown heterostructure, and this was also observed for the different MoS_2 coverage, even with a graphene domain partially covered with MoS_2 crystals (see Figure S5, Supporting Information). The optical response increases with the power density of the laser light as can be seen in Figure S7, Supporting Information, and we could observe the photoinduced current modulation even at 1.4 W/m^2.

CONCLUSIONS

In the present paper, the CVD growth of monolayer MoS_2 crystals on single-crystalline monolayer graphene domains is demonstrated. The single-crystalline MoS_2 domains grow epitaxially on the graphene with orientations defined by the underlying graphene. The controlled orientation and significant PL quenching of monolayer MoS_2 observed in the heterostructure suggest a large effective interlayer coupling due to the direct growth and the reduced interfacial contamination that usually occurs for stacked structures. The direct growth also affected the Raman spectrum of graphene, suggesting effective

DOI: 10.1021/am508569m
ACS Appl. Mater. Interfaces 2015, 7, 5265−5273

van der Waals interaction and/or strain in graphene. We observed photoinduced electron transfer from MoS_2 to graphene and demonstrated the optical memory effect using the MoS_2–graphene hybrid. Our work indicates the possible synthesis of epitaxial heterostructures by CVD, which can ensure the effective interlayer interaction, thus enhancing the potential applications in electronic, optoelectronic, and chemical fields.

EXPERIMENTAL SECTION

Sample Preparation. We used a Cu(111) film deposited on sapphire *c*-plane as catalyst to grow hexagonal graphene domains. Monolayer graphene (MLG) was grown by ambient pressure CVD with CH_4, H_2, and Ar gases at 1075 °C.[32] For the transfer from the Cu(111) film, the graphene surface was covered with a PMMA film by spin coating. After removing the Cu film by immersing in an aqueous solution of ammonium persulfate ($(NH_4)_2S_2O_8$), the PMMA/graphene stack was transferred onto a SiO_2/Si substrate. Finally, the PMMA film was removed by dipping the substrate into acetone solution.[32]

MoS_2 was grown using MoO_3 and S powder (both from Sigma-Aldrich) by ambient pressure CVD using a three-zone furnace equipped with a quartz tube. The CVD setup is illustrated in Figure S1, Supporting Information. The typical temperatures of MoO_3 and S powder were 630–650 and 165 °C, respectively. Pure Ar gas (99.999%) was used as the carrier gas. Graphene/SiO_2/Si or sapphire substrates were placed in the middle of the furnace. The growth time was set 60 min. The final surface coverage of MoS_2 depends on the position of the substrate and the temperature of MoO_3. MoS_2 crystals grown preferentially on the CVD-grown graphene transferred on SiO_2/Si substrates. The temperature of the graphene/SiO_2/Si substrates was set at 900–960 °C. MoS_2 crystals were also grown on sapphire *c*-plane (α-Al_2O_3 (0001)) substrates. For comparison, the MoS_2 domains grown on sapphire were also transferred onto SiO_2/Si surface by a similar method (i.e., PMMA-assisted transfer) used for graphene transfer.

Characterization. Scanning electron microscopy (SEM, HITACHI S-4800) and atomic force microscopy (AFM, Bruker Nanoscope V) were used to image MoS_2 and graphene. Raman and PL spectra and mapping images were measured with a Nanofinder30 (Tokyo Instruments) using a 532 nm excitation. TEM images were measured with a FEI Titan with an acceleration voltage of 200 kV. FETs were made by photolithography, Au metal evaporation, and lift-off processes and measured by semiconductor parameter analyzer (B1500A, Keysight Technologies) in vacuum (typically 3×10^{-4} Pa). Photoinduced current modulation was measured by illuminating a device with a 532 nm laser whose spot size is expanded to ~6.4 mm diameter, and power densities were controlled by using optical filters. The typical power of the illuminating laser was 4.53 mW when an optical filter (optical density (OD) = 1) was used (140 W/m^2). The experimental setup for the photoinduced FET measurement is illustrated in Figure S8, Supporting Information.

ASSOCIATED CONTENT

Supporting Information

Experimental setup for MoS_2 growth, SEM images of MoS_2–graphene heterostructure with different MoS_2 coverages, AFM and Raman data of annealed graphene domains, CVD result of the graphene/Cu/sapphire substrate, photoresponse of other devices, laser power dependence, and setup of photoinduced carrier modulation experiment. This material is available free of charge via the Internet at http://pubs.acs.org.

AUTHOR INFORMATION

Corresponding Author

*E-mail: ago@cm.kyushu-u.ac.jp.

Notes

The authors declare no competing financial interest.

ACKNOWLEDGMENTS

This work was supported by PRESTO-JST. P.S.F. acknowledges the receipt of a postdoctoral Fellowship from JSPS.

REFERENCES

(1) Wang, Q. H.; Kalantar-Zadeh, K.; Kis, A.; Coleman, J. N.; Strano, M. S. Electronics and Optoelectronics of Two-Dimensional Transition Metal Dichalcogenides. *Nat. Nanotechnol.* **2012**, *7*, 699–712.

(2) Chhowalla, M.; Shin, H. S.; Eda, G.; Li, L.-J.; Loh, K. P.; Zhang, H. The Chemistry of Two-Dimensional Layered Transition Metal Dichalcogenide Nanosheets. *Nat. Chem.* **2013**, *5*, 263–275.

(3) Butler, S. Z.; Hollen, S. M.; Cao, L.; Cui, Y.; Gupta, J. A.; Gutiérrez, H. R.; Heinz, T. F.; Hong, S. S.; Huang, J.; Ismach, A. F.; Johnston-Halperin, E.; Kuno, M.; Plashnitsa, V. V.; Robinson, R. D.; Ruoff, R. S.; Salahuddin, S.; Shan, J.; Shi, L.; Spencer, M. G.; Terrones, M.; Windl, W.; Goldberger, J. E. Progress, Challenges, and Opportunities in Two-Dimensional Materials Beyond Graphene. *ACS Nano* **2013**, *7*, 2898–2926.

(4) Xu, M.; Liang, T.; Shi, M.; Chen, H. Graphene-Like Two-Dimensional Materials. *Chem. Rev.* **2013**, *113*, 3766–3798.

(5) Li, L.; Yu, Y.; Ye, G. J.; Ge, Q.; Ou, X.; Wu, H.; Feng, D.; Chen, X. H.; Zhang, Y. Black Phosphorus Field-Effect Transistors. *Nat. Nanotechnol.* **2014**, *9*, 372–377.

(6) Lim, H.; Yoon, S. I.; Kim, G.; Jang, A.-R.; Shin, H. S. Stacking of Two-Dimensional Materials in Lateral and Vertical Directions. *Chem. Mater.* **2014**, *26*, 4891–4903.

(7) Lee, G.-H.; Yu, Y.-J.; Cui, X.; Petrone, N.; Lee, C.-H.; Choi, M. S.; Lee, D.-Y.; Lee, C.; Yoo, W. J.; Watanabe, K.; Taniguchi, T.; Nuckolls, C.; Kim, P.; Hone, J. Flexible and Transparent MoS_2 Field-Effect Transistors on Hexagonal Boron Nitride-Graphene Heterostructures. *ACS Nano* **2013**, *7*, 7931–7936.

(8) Biswas, C.; Lee, Y. H. Graphene Versus Carbon Nanotubes in Electronic Devices. *Adv. Funct. Mater.* **2011**, *21*, 3806–3826.

(9) Nair, R. R.; Blake, P.; Grigorenko, A. N.; Novoselov, K. S.; Booth, T. J.; Stauber, T.; Peres, N. M. R.; Geim, A. K. Fine Structure Constant Defines Visual Transparency of Graphene. *Science* **2008**, *320*, 1308.

(10) Eda, G.; Yamaguchi, H.; Voiry, D.; Fujita, T.; Chen, M.; Chhowalla, M. Photoluminescence from Chemically Exfoliated MoS_2. *Nano Lett.* **2011**, *11*, 5111–5116.

(11) Mak, K. F.; Lee, C.; Hone, J.; Shan, J.; Heinz, T. F. Atomically Thin MoS_2: A New Direct-Gap Semiconductor. *Phys. Rev. Lett.* **2010**, *105*, 136805.

(12) Radisavljevic, B.; Radenovic, A.; Brivio, J.; Giacometti, V.; Kis, A. Single-Layer MoS_2 Transistors. *Nat. Nanotechnol.* **2011**, *6*, 147–150.

(13) Zhang, W.; Chuu, C.-P.; Huang, J.-K.; Chen, C.-H.; Tsai, M.-L.; Chang, Y.-H.; Liang, C.-T.; Chen, Y.-Z.; Chueh, Y.-L.; He, J.-H.; Chou, M.-Y.; Li, L.-J. Ultrahigh-Gain Photodetectors Based on Atomically Thin Graphene-MoS_2 Heterostructures. *Sci. Rep.* **2014**, *4*, 3826.

(14) Roy, K.; Padmanabhan, M.; Goswami, S.; Sai, T. P.; Ramalingam, G.; Raghavan, S.; Ghosh, A. Graphene-MoS_2 Hybrid Structures for Multifunctional Photoresponsive Memory Devices. *Nat. Nanotechnol.* **2013**, *8*, 826–830.

(15) Yu, W. J.; Liu, Y.; Zhou, H.; Yin, A.; Li, Zheng; Huang, Y.; Duan, X. Highly Efficient Gate-Tunable Photocurrent Generation in Vertical Heterostructures of Layered Materials. *Nat. Nanotechnol.* **2013**, *8*, 952–958.

(16) Yu, W. J.; Li, Z.; Zhou, H.; Chen, Y.; Wang, Y.; Huang, Y.; Duan, X. Vertically Stacked Multi-Heterostructures of Layered Materials for Logic Transistors and Complementary Inverters. *Nat. Mater.* **2013**, *12*, 246–252.

(17) Bertolazzi, S.; Krasnozhon, D.; Kis, A. Nonvolatile Memory Cells Based on MoS_2/Graphene Heterostructures. *ACS Nano* **2013**, *7*, 3246–3252.

(18) Shih, C.-J.; Wang, Q. H.; Son, Y.; Jin, Z.; Blankschtein, D.; Strano, M. S. Tuning On-Off Current Ratio and Field-Effect Mobility

DOI: 10.1021/am508569m
ACS Appl. Mater. Interfaces 2015, 7, 5265–5273

in a MoS_2-Graphene Heterostructure via Schottky Barrier Modulation. *ACS Nano* **2014**, *8*, 5790−5798.
(19) Diaz, H. C.; Addou, R.; Batzill, M. Interface Properties of CVD Grown Graphene Transferred onto MoS_2(0001). *Nanoscale* **2014**, *6*, 1071−1078.
(20) Liu, K.-K.; Zhang, W.; Lee, Y.-H.; Lin, Y.-C.; Chang, M.-T.; Su, C.-Y.; Chang, C.-S.; Li, H.; Shi, Y.; Zhang, H.; Lai, C.-S.; Li, L.-J. Growth of Large-Area and Highly Crystalline MoS_2 Thin Layers on Insulating Substrates. *Nano Lett.* **2012**, *12*, 1538−1544.
(21) Zhang, Y.; Liu, Z.; Najmaei, S.; Ajayan, P. M.; Lou, J. Large-Area Vapor-Phase Growth and Characterization of MoS_2 Atomic Layers on a SiO_2 Substrate. *Small* **2011**, *8*, 966−971.
(22) van der Zande, A. M.; Huang, P. Y.; Chenet, D. A.; Berkelbach, T. C.; You, Y.; Lee, G.-H.; Heinz, T. F.; Reichman, D. R.; Muller, D. A.; Hone, J. C. Grains and Grain Boundaries in Highly Crystalline Monolayer Molybdenum Disulphide. *Nat. Mater.* **2013**, *12*, 554−561.
(23) Haigh, S. J.; Gholinia, A.; Jalil, R.; Romani, S.; Britnell, L.; Elias, D. C.; Novoselov, K. S.; Ponomarenko, L. A.; Geim, A. K.; Gorbachev, R. Cross-Sectional Imaging of Individual Layers and Buried Interfaces of Graphene-Based Heterostructures and Superlattices. *Nat. Mater.* **2012**, *11*, 764−767.
(24) Lin, Y.-F.; Li, W.; Li, S.-L.; Xu, Y.; Aparecido-Ferreira, A.; Komatsu, K.; Sun, H.; Nakaharai, S.; Tsukagoshi, K. Barrier Inhomogeneities at Vertically Stacked Graphene-based Heterostructures. *Nanoscale* **2014**, *6*, 795−799.
(25) Shi, Y.; Zhou, W.; Lu, A.-Y.; Fang, W.; Lee, Y.-H.; Hsu, A. L.; Kim, S. M.; Kim, K. K.; Yang, H. Y.; Li, L.-J.; Idrobo, J.-C.; Kong, J. van der Waals Epitaxy of MoS_2 Layers Using Graphene As Growth Templates. *Nano Lett.* **2012**, *12*, 2784−2791.
(26) Ling, X.; Lee, Y.-H.; Lin, Y.; Fang, W.; Yu, L.; Dresselhaus, M. S.; Kong, J. Role of the Seeding Promoter in MoS_2 Growth by Chemical Vapor Deposition. *Nano Lett.* **2014**, *14*, 464−472.
(27) Lin, Y.-C.; Lu, N.; Perea-Lopez, N.; Li, J.; Lin, Z.; Peng, X.; Lee, C. H.; Sun, C.; Calderin, L.; Browning, P. N.; Bresnehan, M. S.; Kim, M. J.; Mayer, T. S.; Terrones, M.; Robinson, J. A. Direct Synthesis of van der Waals Solids. *ACS Nano* **2014**, *8*, 3715−3723.
(28) Shim, G. W.; Yoo, K.; Seo, S.-B.; Shin, J.; Jung, D. Y.; Kang, I.-S.; Ahn, C. W.; Cho, B. J.; Choi, S.-Y. Large-Area Single-Layer $MoSe_2$ and Its van der Waals Heterostructures. *ACS Nano* **2014**, *8*, 6655−6662.
(29) Okada, M.; Sawazaki, T.; Watanabe, K.; Taniguchi, T.; Hibino, H.; Shinohara, H.; Kitaura, R. Direct Chemical Vapor Deposition Growth of WS_2 Atomic Layers on Hexagonal Boron Nitride. *ACS Nano* **2014**, *8*, 8273−8277.
(30) Kim, J.; Bayram, C.; Park, H.; Cheng, C.-W.; Dimitrakopoulos, C.; Ott, J. A.; Reuter, K. B.; Bedell, S. W.; Sadana, D. K. Principle of Direct van der Waals Epitaxy of Single-Crystalline Films on Epitaxial Graphene. *Nat. Commun.* **2014**, *5*, 4836.
(31) Mohseni, P. K.; Behnam, A.; Wood, J. D.; English, C. D.; Lyding, J. W.; Pop, E.; Li, X. $In_xGa_{1-x}As$ Nanowire Growth on Graphene: van der Waals Epitaxy Induced Phase Segregation. *Nano Lett.* **2013**, *13*, 1153−1161.
(32) Ago, H.; Kawahara, K.; Ogawa, Y.; Tanoue, S.; Bissett, M. A.; Tsuji, M.; Sakaguchi, H.; Koch, R. J.; Fromm, F.; Seyller, T.; Komatsu, K.; Tsukaghoshi, K. Epitaxial Growth and Electronic Properties of Large Hexagonal Graphene Domains on Cu(111) Thin Film. *Appl. Phys. Express* **2013**, *6*, 75101.
(33) Lee, Y.-H.; Zhang, X.-Q.; Zhang, W.; Chang, M.-T.; Lin, C.-T.; Chang, K.-D.; Yu, Y.-C.; Wang, J. T.-W.; Chang, C.-S; Li, L.-J.; Lin, T.-W. Synthesis of Large-Area MoS_2 Atomic Layers with Chemical Vapor Deposition. *Adv. Mater.* **2014**, *24*, 2320−2325.
(34) Dumcenco, D.; Ovchinnikov, D.; Marinov, K.; Lopez-Sanchez, O.; Krasnozhon, D.; Chen, M.-W.; Gillet, P.; Morral, A. F.; Radenovic, A.; Kis, A. Large-Area Epitaxial Monolayer MoS_2. arXiv: 1405.0129 [cond-mat.-mes-hall].
(35) Wu, S.; Huang, C.; Aivazian, G.; Ross, J. S.; Cobden, D. H.; Xu, X. Vapor-Solid Growth of High Optical Quality MoS_2 Monolayers with Near-Unity Valley Polarization. *ACS Nano* **2013**, *7*, 2768−2772.
(36) Ji, Q.; Kan, M.; Zhang, Y.; Guo, Y.; Ma, D.; Shi, J.; Sun, Q.; Chen, Q.; Zhang, Y.; Liu, Z. Unravelling Orientation Distribution and Merging Behavior of Monolayer MoS_2 Domains on Sapphire. *Nano Lett.* **2015**, *15*, 198−205.
(37) Ferrari, A. C.; Meyer, J. C.; Scardaci, V.; Casiraghi, C.; Lazzeri, M.; Mauri, F.; Piscanec, S.; Jiang, D.; Novoselov, K. S.; Roth, S.; Geim, A. K. Raman Spectrum of Graphene and Graphene Layers. *Phys. Rev. Lett.* **2006**, *97*, 187401.
(38) Nourbakhsh, A.; Cantoro, M.; Klekachev, A.; Clemente, F.; Sorée, B.; van der Veen, M. H.; Vosch, T.; Stesmans, A.; Sels, B.; De Gendt, S. Tuning the Fermi Level of SiO_2-Supported Single-Layer Graphene by Thermal Annealing. *J. Phys. Chem. C* **2010**, *114*, 6894−6900.
(39) Calizo, I.; Ghosh, S.; Bao, W.; Miao, F.; Lau, C. N.; Balandin, A. A. Raman Nanometrology of Graphene: Temperature and Substrate Effects. *Solid State Commun.* **2009**, *149*, 1132−1135.
(40) Ferrari, A. C. Raman Spectroscopy of Graphene and Graphite: Disorder, Electron-Phonon Coupling, Doping and Nonadiabatic Effects. *Solid State Commun.* **2007**, *143*, 47−57.
(41) Das, A.; Pisana, S.; Chakraborty, B.; Piscanec, S.; Saha, S. K.; Waghmare, U. V.; Novoselov, K. S.; Krishnamurthy, H. R.; Geim, A. K.; Ferrari, A. C.; Sood, A. K. Monitoring Dopants by Raman Scattering in an Electrochemically Top-Gated Graphene Transistor. *Nat. Nanotechnol.* **2008**, *3*, 210−215.
(42) Bissett, M. A.; Konabe, S.; Okada, S.; Tsuji, M.; Ago, H. Enhanced Chemical Reactivity of Graphene Induced by Mechanical Strain. *ACS Nano* **2013**, *7*, 10335−10343.
(43) Huang, M.; Yan, H.; Heinz, T. F.; Hone, J. Probing Strain-Induced Electronic Structure Change in Graphene by Raman Spectroscopy. *Nano Lett.* **2010**, *10*, 4074−4079.
(44) Bissett, M. A.; Tsuji, M.; Ago, H. Strain Engineering the Properties of Graphene and Other Two-Dimensional Crystals. *Phys. Chem. Chem. Phys.* **2014**, *16*, 11124−11138.
(45) Zhou, K.-G.; Withers, F.; Cao, Y.; Hu, S.; Yu, G.; Casiraghi, C. Raman Modes of MoS_2 Used as Fingerprint of van der Waals Interactions in 2-D Crystal-Based Heterostructures. *ACS Nano* **2014**, *8*, 9914−9924.
(46) El-Mahalawy, S. H.; Evans, B. L. The Thermal Expansion of 2H-MoS_2, 2H-$MoSe_2$ and 2H-WSe_2 between 20 and 800 °C. *J. Appl. Crystallogr.* **1976**, *9*, 403−406.
(47) Yoon, D.; Son, Y.-W.; Cheong, H. Negative Thermal Expansion Coefficient of Graphene Measured by Raman Spectroscopy. *Nano Lett.* **2011**, *11*, 3227−3231.
(48) Bissett, M. A.; Izumida, W.; Saito, R.; Ago, H. Effect of Domain Boundaries on the Raman Spectra of Mechanically Strained Graphene. *ACS Nano* **2012**, *6*, 10229−10238.

DOI: 10.1021/am508569m
ACS Appl. Mater. Interfaces 2015, 7, 5265−5273